

REPORT DOCUMENTATION PAGE

Form Approved
OMB No. 0704-0188

Public reporting burden for this collection of information is estimated to average 1 hour per response, including the time for reviewing instructions, searching existing data sources, gathering and maintaining the data needed, and completing and reviewing this collection of information. Send comments regarding this burden estimate or any other aspect of this collection of information, including suggestions for reducing this burden to Department of Defense, Washington Headquarters Services, Directorate for Information Operations and Reports (0704-0188), 1215 Jefferson Davis Highway, Suite 1204, Arlington, VA 22202-4302. Respondents should be aware that notwithstanding any other provision of law, no person shall be subject to any penalty for failing to comply with a collection of information if it does not display a currently valid OMB control number. **PLEASE DO NOT RETURN YOUR FORM TO THE ABOVE ADDRESS.**

| | | | | | |
|---|--------------------|--|-----------------------------------|---|--|
| 1. REPORT DATE (DD-MM-YYYY) 25-08-2009 | | 2. REPORT TYPE Technical Paper | | 3. DATES COVERED (From - To) | |
| 4. TITLE AND SUBTITLE Laser- Induced Fluorescence Velocity Measurements of a Low Power Cylindrical Hall Thruster | | | | 5a. CONTRACT NUMBER | |
| | | | | 5b. GRANT NUMBER | |
| | | | | 5c. PROGRAM ELEMENT NUMBER | |
| 6. AUTHOR(S) Natalia A. MacDonald & Mark A. Capelli (Stanford); William A. Hargus Jr (AFRL/RZSS) | | | | 5d. PROJECT NUMBER | |
| | | | | 5e. TASK NUMBER | |
| | | | | 5f. WORK UNIT NUMBER 33SP0706 | |
| 7. PERFORMING ORGANIZATION NAME(S) AND ADDRESS(ES) Air Force Research Laboratory (AFMC) AFRL/RZST 4 Draco Drive Edwards AFB CA 93524-7160 | | | | 8. PERFORMING ORGANIZATION REPORT NUMBER AFRL-RZ-ED-TP-2009-321 | |
| 9. SPONSORING / MONITORING AGENCY NAME(S) AND ADDRESS(ES) Air Force Research Laboratory (AFMC) AFRL/RZS 5 Pollux Drive Edwards AFB CA 93524-7048 | | | | 10. SPONSOR/MONITOR'S ACRONYM(S) | |
| | | | | 11. SPONSOR/MONITOR'S NUMBER(S) AFRL-RZ-ED-TP-2009-321 | |
| 12. DISTRIBUTION / AVAILABILITY STATEMENT Approved for public release; distribution unlimited (PA #09398). | | | | | |
| 13. SUPPLEMENTARY NOTES For 31 st International Electric Propulsion Conference (IEPC 09) to be held in Ann Arbor, MI from 20-24 September 2009. | | | | | |
| 14. ABSTRACT This work presents a preliminary survey of the axial velocities within the acceleration channel and axial, radial and azimuthal velocities in the plume of a Princeton University low power cylindrical Hall thruster. Xenon ion velocities for the thruster are derived from laser-induced fluorescence measurements of the 5d[4] _{7/2} -6p[3] _{5/2} xenon ion excited state transition. Three operating conditions are considered with variations to the magnetic field strength and chamber background pressure in an effort to capture their effects on ion acceleration and centerline ion energy distributions. Under nominal conditions, xenon ions are accelerated to an energy of 25 eV within the thruster with an additional 188 eV gain in the thruster plume. At a position 40 mm into the plume, this constitutes an energy of 213 eV at an applied potential of 300 V. Decreasing the magnetic field strength appears to reduce the magnitude of radial ion velocities and pushes the peak electric field downstream into the plume. Increasing the background pressure is shown to reduce the plume divergence, move the peak electric field upstream towards the thruster exit plane, and result in a higher centerline axial ion velocity in the far-field of the plume. | | | | | |
| 15. SUBJECT TERMS | | | | | |
| 16. SECURITY CLASSIFICATION OF: | | | 17. LIMITATION OF ABSTRACT | 18. NUMBER OF PAGES | 19a. NAME OF RESPONSIBLE PERSON |
| a. REPORT | b. ABSTRACT | c. THIS PAGE | | | Dr. William A. Hargus Jr |
| Unclassified | Unclassified | Unclassified | SAR | 29 | 19b. TELEPHONE NUMBER (include area code) N/A |

Laser-Induced Fluorescence Velocity Measurements of a Low Power Cylindrical Hall Thruster

Natalia A. MacDonald and Mark A. Cappelli
Stanford Plasma Physics Laboratory
Stanford University
Stanford, CA 94305

William A. Hargus, Jr.
Spacecraft Propulsion Branch
Air Force Research Laboratory
Edwards AFB, CA 93524

This work presents a preliminary survey of the axial velocities within the acceleration channel and axial, radial and azimuthal velocities in the plume of a Princeton University low power cylindrical Hall thruster. Xenon ion velocities for the thruster are derived from laser-induced fluorescence measurements of the $5d[4]_{7/2} - 6p[3]_{5/2}$ xenon ion excited state transition. Three operating conditions are considered with variations to the magnetic field strength and chamber background pressure in an effort to capture their effects on ion acceleration and centerline ion energy distributions. Under nominal conditions, xenon ions are accelerated to an energy of 25 eV within the thruster with an additional 188 eV gain in the thruster plume. At a position 40 mm into the plume, this constitutes an energy of 213 eV at an applied potential of 300 V. Decreasing the magnetic field strength appears to reduce the magnitude of radial ion velocities and pushes the peak electric field downstream into the plume. Increasing the background pressure is shown to reduce the plume divergence, move the peak electric field upstream towards the thruster exit plane, and result in a higher centerline axial ion velocity in the far-field of the plume.

Introduction

This study characterizes xenon ion velocities both inside the acceleration channel and in the plume of a low power cylindrical Hall thruster (CHT) using laser-induced fluorescence (LIF). LIF measurements are also used to assess the effect of varying magnetic field strength and background chamber pressure on the evolution of the ion velocity profiles and ion acceleration.

The electrostatic thruster used in this study is the Princeton University CHT-30. The CHT is of interest due to its lack of a protruding central magnetic pole. Previous efforts examining low power annular Hall effect thrusters have shown that erosion of the insulator protecting the central magnetic pole limits thruster lifetime significantly, even more so than erosion of the outer insulator. This effect is amplified

as the power and size of the Hall thruster is scaled down. By reducing the length of the central magnetic pole and creating a region of the channel with a low surface-to-volume area (a cylindrical region), the CHT as developed by Princeton University reduces the impact of insulator erosion significantly.

The CHT-30 has a cylindrical acceleration channel with a diameter of 30 mm and depth of 13 mm. This is similar to most modern Hall thrusters, which have acceleration channels with a maximum depth of 10-20 mm. With this geometry, it is possible to align collection optics to the probe beam such that limited internal optical access is possible without modification. In this work, the collection lens is placed 60° off the plume axis.¹ With the CHT's plume divergence half angle of approximately 60° to 80° ,² this places the collection optics away from much of the plume ion flux. In this way, it is possible to probe in-

ternal ion acceleration of the CHT-30 with minimal intrusion into the plume.

Three thruster operating conditions are examined in this study. These include an nominal condition for which there is unpublished performance data, an off-nominal condition with reduced magnetic field strength, and the off-nominal case at a high background pressure. The goals of these measurements are to characterize the ion velocity for a known case, examine a low plasma oscillation case where the signal-to-noise ratio (SNR) of the diagnostic is maximized, and then look at the behavior of the propellant acceleration under high background pressure to examine the thruster's sensitivity to chamber effects.

Experimental Apparatus

Xenon Ion Spectroscopy

For the results reported here, the $5d[4]_{7/2} - 6p[3]_{5/2}$ electronic transition of Xe II at 834.7 nm is probed. The isotopic and nuclear-spin effects contributing to the hyperfine structure of the $5d[4]_{7/2} - 6p[3]_{5/2}$ xenon ion transition produce a total of 19 isotopic and spin split components. The hyperfine splitting constants which characterize the variations in state energies are only known for a limited set of energy levels. Unfortunately, this xenon ion transition only has confirmed data on the nuclear spin splitting constants of the $6p[3]_{5/2}$ upper state.³⁻⁶

Manzella first used the $5d[4]_{7/2} - 6p[3]_{5/2}$ xenon ion transition at 834.7 nm to make velocity measurements in a Hall thruster plume.⁷ A convenient feature of this transition is the presence of a relatively strong line originating from the same upper state ($6s[2]_{3/2} - 6p[3]_{5/2}$ transition at 541.9 nm,⁸ which allows for non-resonant fluorescence collection). Ion velocity is simply determined by measurement of the Doppler shift of the absorbing ions.⁹

Test Facility

The LIF measurements were performed in Chamber 6 of the Air Force Research Laboratory (AFRL) Electric Propulsion Laboratory at Edwards AFB, CA. Chamber 6 is a non-magnetic stainless steel chamber with a 1.8 m diameter and 3 m length. It has a measured pumping speed of 32,000 L/s on xenon. Pumping is provided by four single stage cryogenic panels (single stage cold heads at 25 K) and one 50 cm two stage cryogenic pump (12 K). Chamber pressure during thruster operation is approximately 2.8×10^{-6} torr, corrected for xenon.

Figure 1 shows a top view of the laser optical

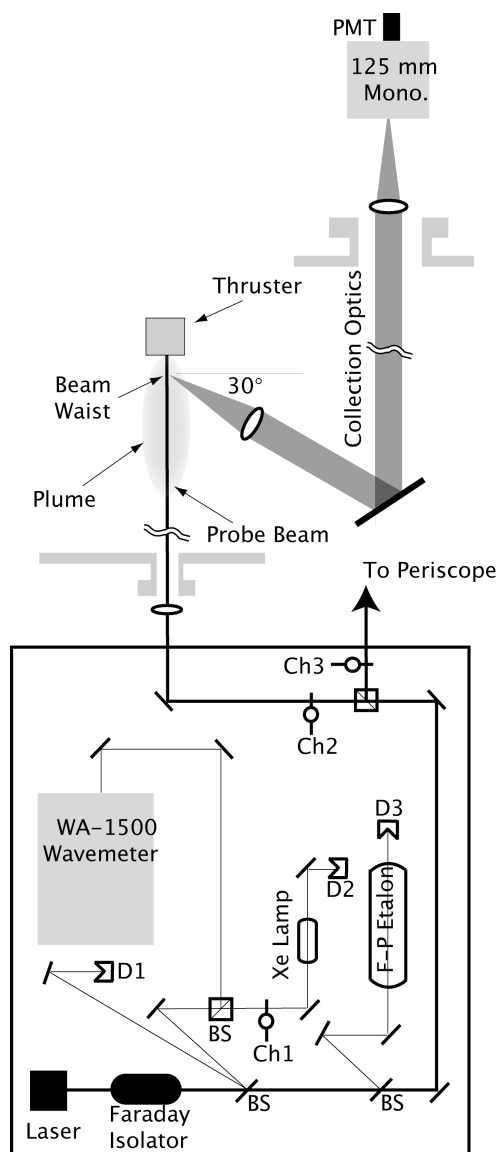


Figure 1. Top view diagram of the laser optical train and collection optics. Note that the radial probe beam periscope and focusing optics are not shown.

train, collection optics, and one leg of the external probe optics. The laser is a tunable diode laser, capable of tuning approximately ± 50 GHz about a center wavelength of 834.7 nm. The 10 mW beam is passed through a Faraday isolator to eliminate feedback to the laser. The laser beam then passes through several beam pick-offs followed by a 50-50 cube beam splitter where it is split into two beams of equal power. The first beam, the axial probe beam shown in Figures 1 and 2 is focused by a lens and enters the vacuum chamber through a window. A second probe beam, shown in Figure 2 only, is directed from the optical bench via a periscope apparatus so that it enters the chamber from above the thruster and probes

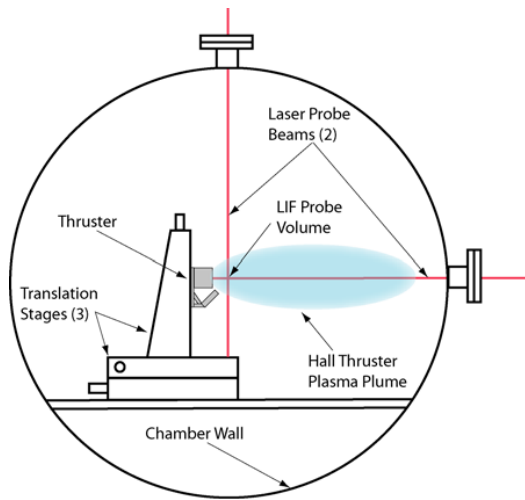


Figure 2. Side view diagram of thruster within AFRL chamber 6. Also shown are the translation stages and the laser probe beams. Note that the fluorescence collection and external optics are not shown.

the velocity perpendicular to the first probe beam. Each probe beam is chopped at a unique frequency by choppers Ch2 (2kHz) and Ch3 (2.8 kHz) for phase sensitive detection of the fluorescence signals.

The two wedge beam pick-offs (BS) shown in Figure 1 provide portions of the beam for diagnostic purposes. The first beam pick-off directs a beam to a photodiode detector (D1) used to provide constant power feedback to the laser. The second beam is divided into two equal components by a 50-50 cube beam splitter. The first component is directed to a commercial wavelength meter used to monitor absolute wavelength. The second component is sent through an optical chopper (Ch1 at 1.4 kHz) and through a low pressure xenon hollow cathode discharge lamp. The lamp provides a stationary absorption reference for the determination of the Doppler shift. Unfortunately, there is no detectable population of the ionic xenon $5d[4]_{7/2}$ state. However, there is a nearby (estimated to be 18.1 GHz distant) neutral xenon $6s'[1/2]_1 - 6p'[3/2]_2$ transition at 834.68 nm.^{10,11} The second pick-off sends a beam to a 300 MHz free spectral range Fabry-Perot etalon (F-P) that provides high resolution frequency monitoring of the wavelength interval swept during a laser scan.

The fluorescence collection optics are also shown in Figure 1. The fluorescence is collected by a 75 mm diameter, 300 mm focal length lens within the chamber and oriented 60° from the probe beam axis. The collimated fluorescence signal is directed through a window in the chamber side wall to a similar lens that focuses the collected fluorescence onto the entrance

slit of the 125 mm focal length monochromator with a photomultiplier tube (PMT). Due to the 1:1 magnification of the collection optics, the spatial resolution of the measurements is determined by the geometry of the entrance slit 0.7 mm width and 1.5 mm height as well as the sub-mm diameter of the probe beam. This apparatus allows for limited probing of the interior acceleration channel of Hall thrusters with relatively shallow acceleration channels. Measurements suggest that this combination of apparatus and laser power are well within the linear fluorescence regime.

Figure 3 shows a typical LIF trace. The uncertainty of the velocity measurements is estimated to be within ± 500 m/s. The repeatability of the peak locations appear to be a fraction of the quoted uncertainty. However, the fluorescence line shapes are often significantly broadened, presumably due to wide velocity distributions caused by plasma fluctuations. The quoted uncertainty should therefore be viewed as the uncertainty in the determination of the peak of the fluorescence line shape. In most cases, this will correspond to the velocity of the majority of the ion population.

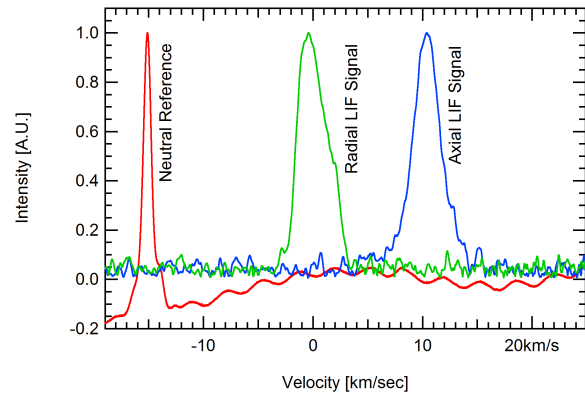


Figure 3. Sample LIF/Absorption trace taken at $Y = +2$ mm, $Z = +10$ mm. Note that the absorption trace has been rectified for clarity.

Cylindrical Hall Thruster

The thruster used in this study is the CHT-30 cylindrical Hall thruster developed by Princeton University. The CHT-30 has a 30 mm diameter channel that is composed of a short annular region near the anode followed by a 13 mm long cylindrical region as shown in Figure 4. CHTs have been of particular interest in the electric propulsion community in recent years due to their low power operation. The low surface-to-volume ratio of their acceleration channel and cusped magnetic field configuration result in low erosion rates of their ceramic wall materials, which is especially desirable when scaling

down in power. CHTs have also demonstrated performance levels similar to state-of-the-art annular Hall thrusters.¹²

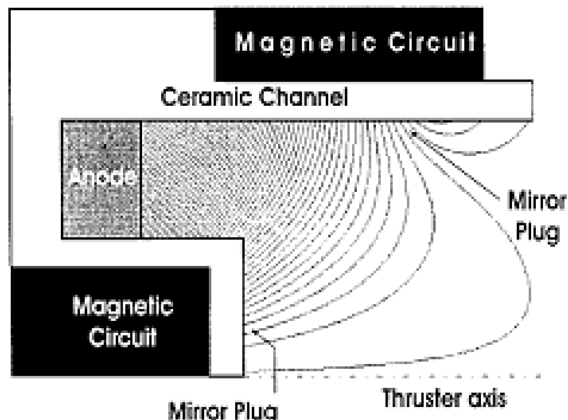


Figure 4. CHT Magnetic field distribution for cusped field configuration.¹³

Although the CHT and several other magnetic cusp electrostatic thrusters have elements that superficially resemble Hall effect thrusters, this thruster type has several features that make it considerably different.¹⁴ First, the high magnetic field strengths within cusp thrusters suggest that the ions may be magnetized. Ion magnetization is understood not to exist in annular Hall thrusters. Furthermore, the geometry and magnetic field structure of cusp thrusters are notably different, with the cusped magnetic field shape seeing no analog in traditional Hall thrusters. In this early stage of research, these differences appear to indicate that the electron transport mechanism within cusp thrusters also differs significantly. The azimuthal $E \times B$ drift seen in conventional Hall thrusters is either lacking or occurs very near the anode of the cusp thruster. This suggests that the $E \times B$ shear that appears critical in annular Hall thruster electron transport does not exist, or assumes a very different form in cusp thrusters. Overall, it appears disingenuous to closely link cusped field thrusters to Hall effect thrusters.

Operating Conditions

The operating conditions considered in this study were a nominal operating condition provided in Table 1, as well as an off-nominal condition provided in Table 2. The off-nominal operating condition was chosen due to the quiescent operating mode of the thruster and the improved fluorescence signal quality. These conditions were run with a chamber background pressure of 2.8×10^{-6} torr. The off-nominal

case was also run at a higher chamber pressure of 1.1×10^{-5} torr as a third operating condition.

Table 1. Nominal CHT-30 operating conditions.

| | |
|------------------|---------------------|
| Anode Flow | 390 $\mu\text{g/s}$ |
| Cathode Flow | 98 $\mu\text{g/s}$ |
| Anode Potential | 300 V |
| Anode Current | 0.53 A |
| Keeper Current | OFF |
| Heater Current | 5.0 A |
| Magnet 1 Current | 3.00 A |
| Magnet 2 Current | 2.00 A |

Table 2. Off-Nominal CHT-30 operating conditions.

| | |
|------------------|---------------------|
| Anode Flow | 390 $\mu\text{g/s}$ |
| Cathode Flow | 150 $\mu\text{g/s}$ |
| Anode Potential | 300 V |
| Anode Current | 0.61 A |
| Keeper Current | 0.30 A |
| Heater Current | 5.0 A |
| Magnet 1 Current | 2.00 A |
| Magnet 2 Current | 2.00 A |

Figure 5 depicts the Cartesian coordinate system used in this experiment. Figures 6 and 7 depict side and top views, respectively, of the thruster channel and plume including the positions of the LIF data points taken. The thruster is mounted on a three axes orthogonal computer controlled translation system which allows for precise movements in the X-, Y- and Z-axes. Measurements at various Y-positions provided radial and axial data. In the plume, LIF data was taken with a 2 mm resolution in the Y-direction from $Y = -16$ to $+16$ mm at axial positions from $Z = 0$ to $Z = +60$ mm. Additional points were taken at $Z = +60$ mm to examine the far-field divergence.

Measurements at various X-positions provided azimuthal and axial data. In the X-direction, plume measurements were taken with a resolution of 4 mm at axial positions from $Z = 0$ to $+40$ mm. Additionally, axial velocities were measured inside the thruster channel with 2 mm resolution in both the X- and Z-directions. The depth at which these data points could be collected was limited by the angle inside the thruster visible to the collection optics (60° from the leading edge of the channel).

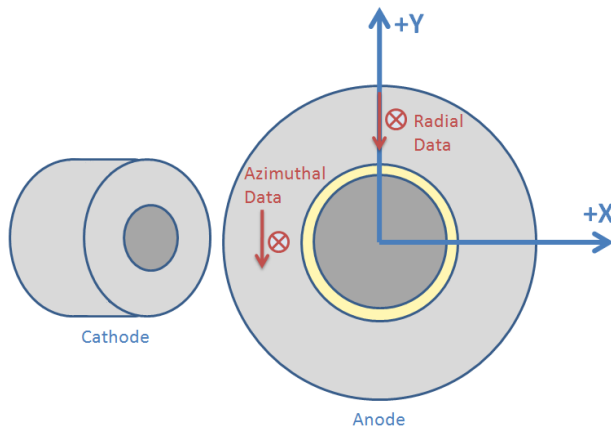


Figure 5. Coordinate system used for data points.

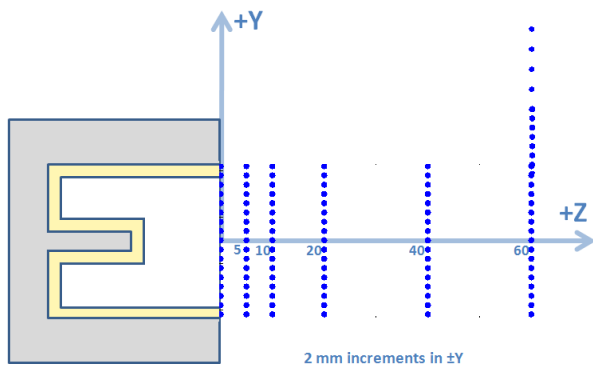


Figure 6. Location of data points for axial and radial LIF measurements.

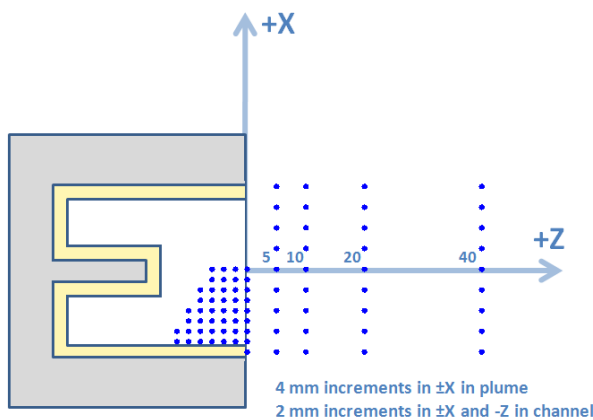


Figure 7. Location of data points for axial and azimuthal LIF measurements.

Results and Discussion

Three operating conditions are considered in this study of the velocity profiles of the CHT-30. Radial

and axial velocities are examined for a nominal operating condition, a condition with reduced magnetic field strength, and the reduced magnetic field case at a higher background pressure. For these conditions, comparisons are made for the centerline velocity and electric field profiles in an effort to see the effects of magnetic field strength and background pressure on the location of peak ion acceleration and maximum achievable ion velocity.

Nominal Operating Condition

Interior Measurements

Due to the constraints of thruster geometry, only axial velocity measurements could be taken without modifying the thruster. These measurements were taken in the X-Z plane only.

Figure 8 is a contour plot of the axial velocities inside the thruster channel under nominal conditions. The ions move more slowly near the channel wall and are accelerated to higher velocities near the centerline of the channel. This could be representative of a convergent ion flux, which is meant to keep energetic ions from hitting the channel walls. The result is a parabolic axial velocity distribution throughout the channel that flattens out to be nearly constant at the exit plane. Within the thruster channel, the minimum measured ion velocity is 850 m/s (0.5 eV) at the channel wall and a depth of -12 mm in the Z-direction. At the exit plane, the maximum ion velocity measured is 6,100 m/s (25 eV) located at the centerline of the channel.

Figure 4 illustrates the cusped magnetic field profile inside a CHT. The magnetic field lines are believed to form equipotential surfaces, creating an electric field that has a significant axial component.¹² Studies performed by Smirnov, et al.,¹⁵ indicate that this electric field profile causes a convergent ion flux, mentioned previously, that focuses the ions towards the centerline of the thruster, keeping them away from the channel walls.¹⁶ This field profile explains the high ion acceleration measured along the centerline of the channel.

Plume Measurements

Figure 9 shows a velocity vector field of singly charged xenon ions in the plume of the CHT-30 under nominal operating conditions. The plume diverges sharply starting at edge of the channel. Due to the lack of center pole piece in the cylindrical design, the plume lacks the prominent mixed flow regime seen in annular Hall thrusters where the ions from opposite sides of the thruster converge.¹⁷

This can be explained by the evolution of the magnetic field profile as it gets farther outside the chan-

nel. The resulting equipotential surfaces provide an electric field profile with a significant outward pointing radial component. From the exit plane outwards into the plume, all radial velocity components are therefore pointing away from the centerline. This plays a large role in the divergence of the plume, and possibly weakens or eliminates the centerline ion flux seen inside the channel, resulting in a reduced mixing zone compared to annular Hall thrusters.

Figure 10 focuses on the radial and axial velocity profiles at the exit plane. The axial velocity is slightly parabolic, with a centerline velocity of 6,100 m/s (25 eV) and an average velocity of 5,300 m/s (19 eV) near the edge of the channel. The ions show most of their acceleration in the radial direction near the edge of the channel at $Y = \pm 10$ mm, reaching a maximum radial velocity of 6,500 m/s (29 eV).

The high radial ion velocity at the exit plane is indicative of the large plume divergence half angle that is typical of cylindrical Hall thrusters. Unlike traditional annular Hall thrusters where the axial component of velocity is much higher than the radial component,¹⁷ at the exit plane, the axial and radial com-

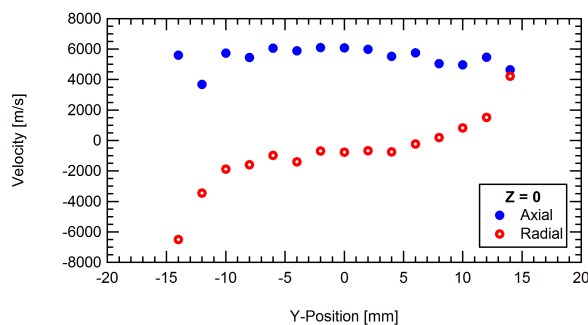


Figure 10. Axial and radial velocity profiles at the exit plane.

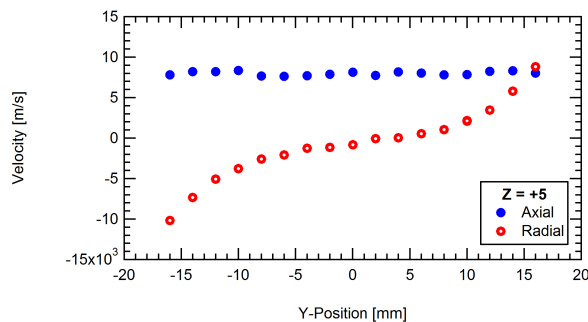


Figure 11. Velocity field at $Z = +5$ mm.

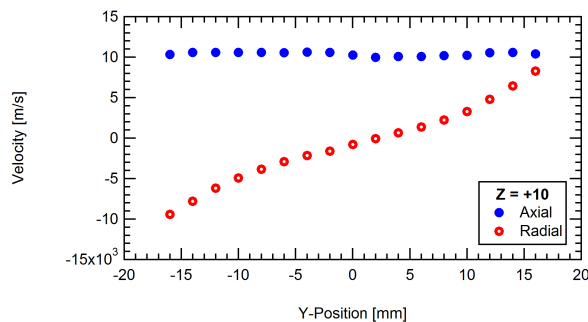


Figure 12. Velocity field at $Z = +10$ mm.

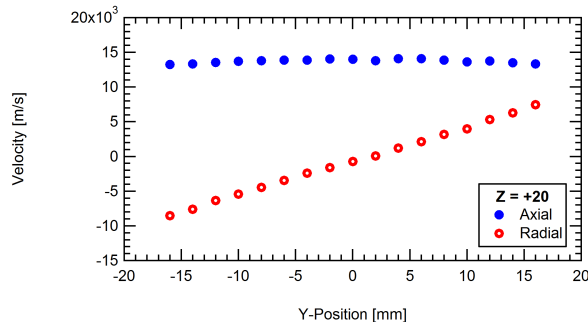


Figure 13. Velocity field at $Z = +20$ mm.

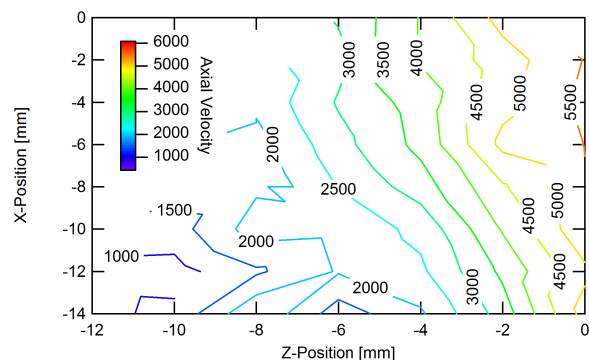


Figure 8. Contour plot of axial velocity (in m/s) inside thruster channel for nominal conditions. Note: the centerline of the thruster is located at the top of the graph at $X = 0$.

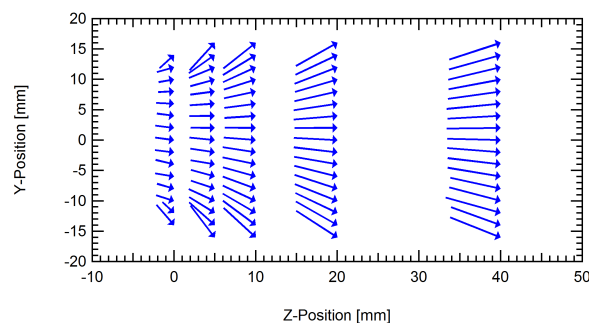


Figure 9. Velocity vector field for nominal condition.

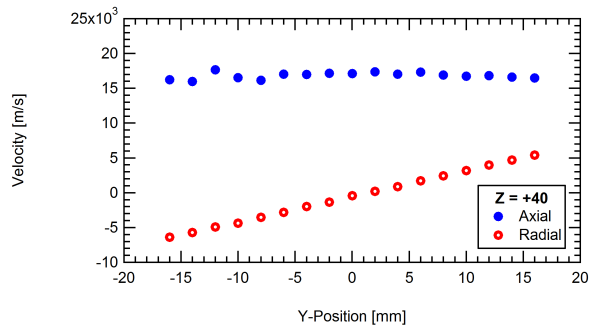


Figure 14. Velocity field at $Z = +40$ mm.

ponents of velocity are nearly the of the same magnitude. Previous studies have shown the half angle of the plume to be as large as 60° to 80° , compared to traditional annular Hall thrusters which have plume divergence half angles of approximately 45° to 50° .² This increased divergence angle could be due to the radial component of the electric field in this region being stronger than that of a traditional annular Hall thruster.¹² It has been suggested that increasing the electron emission from the cathode would reduce the divergence half angle of the plume.¹⁸ This condition was not examined in this study and is left for future LIF experiments.

Figures 11 through 14 depict the evolution of the velocity profiles throughout the plume. Within the uncertainty of the measurements, the axial velocity becomes nearly uniform at distances farther into the plume. The axial velocity increases from 6,100 m/s (25 eV) at the exit plane to 17,700 m/s (213 eV) at $Z = +40$ mm, implying that much of the velocity gained by the ions occurs outside of the thruster channel. This is confirmed by Figure 15 which depicts the centerline ion velocity from inside the thruster channel to a distance of 40 mm into the plume.

As the influence of the magnetic field decreases, the radial velocity distributions become more linear. This is confirmed by Figure 16 which shows the radial electric field profiles flattening out and approaching zero at axial distances greater than $Z = +10$ mm. This is partially a factor of the limited distance from the centerline in which measurements were taken. But it also implies that ions may be magnetized when leaving the thruster channel (causing the large plume divergence half angle), but in the plume, the reduced magnetic field strength allows the ions to continue on relatively straight trajectories once away from the exit plane. Simulations would be necessary to confirm this hypothesis.

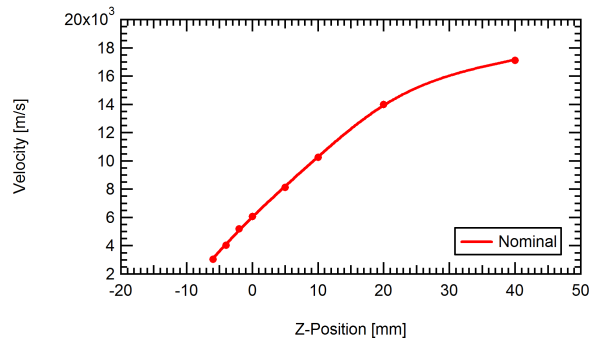


Figure 15. Centerline ion velocity profile for nominal operation.

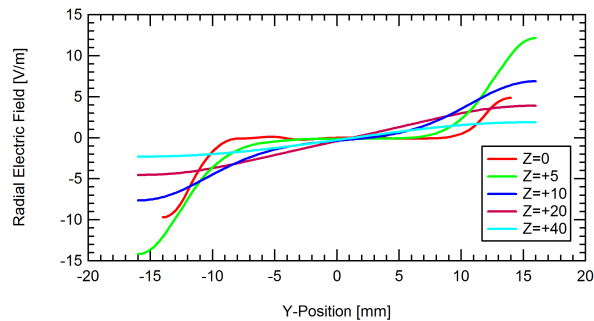


Figure 16. Radial electric field profile for nominal operation.

Off-Nominal Operating Condition

The off-nominal operating condition considered had a lower supplied magnet current. This condition was advantageous because it provided an improved fluorescence signal, and it also gave insight into the influence of the magnetic field strength on the ion velocity profiles.

Interior Measurements

Figure 17 is a contour plot of the axial velocities inside the thruster channel under off-nominal conditions. As was seen in the nominal case, a convergent ion flux forms in the center of the acceleration channel. Also, a parabolic velocity distribution is evident inside the channel, followed by a relatively constant axial velocity across the exit plane.

Qualitatively, both the nominal and off-nominal cases show the similar ion velocity behavior at the low chamber operating pressure. Figure 18 depicts the difference in ion velocity inside the thruster chamber between the nominal and off-nominal conditions. For the majority of the channel, the nominal and off-nominal velocities are within ± 200 m/s. There are some interesting features closer to the channel wall where ions under the nominal condition appear to

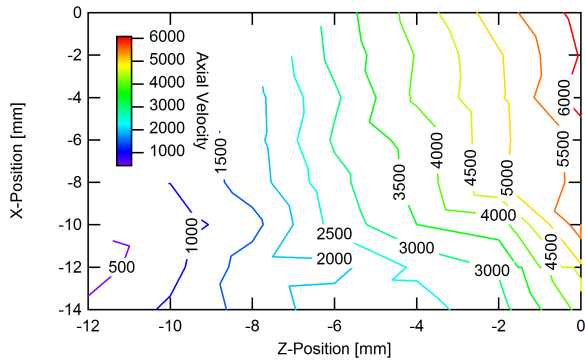


Figure 17. Contour plot of axial velocity (in m/s) inside thruster channel for off-nominal conditions. Note: the centerline of the thruster is located at the top of the graph at $X = 0$.

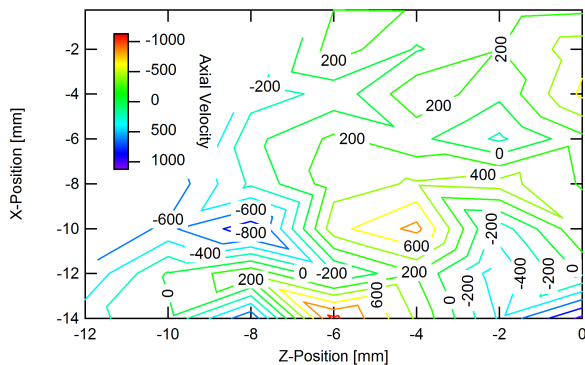


Figure 18. Contour plot of the difference in axial velocity (in m/s) inside thruster channel between nominal and off-nominal conditions. Note: the centerline of the thruster is located at the top of the graph at $X = 0$.

be moving slightly faster at positions closer to the anode ($Z = -8$ to -12 mm), with a difference of 600 to 800 m/s (0.25 to 0.45 eV). At a position of $Z = -6$ mm, however, the ions under the off-nominal condition are moving 600 m/s (0.57 eV) faster. This implies that changing the magnetic field strengths also changes the topology of the magnetic field profile inside the thruster.

Overall, the off-nominal condition with lower magnetic field achieves a slightly higher axial velocity at the exit plane than the nominal case (6,100 m/s (25 eV) nominal vs. 6,600 m/s (30 eV) off-nominal). However, within the uncertainty of the measurements, the peak measured radial velocities are the same for both operating conditions, approximately 6,500 m/s (29 eV) at the edge of the channel.

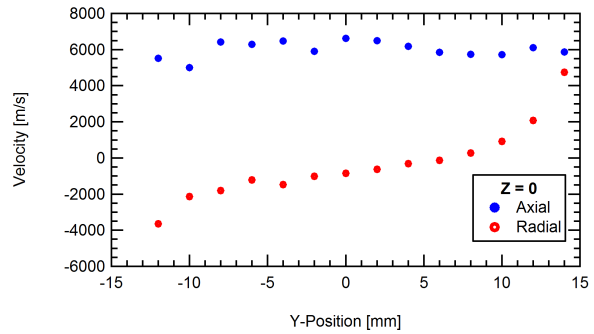


Figure 19. Axial and radial velocity profiles at exit plane for the off-nominal operating condition.

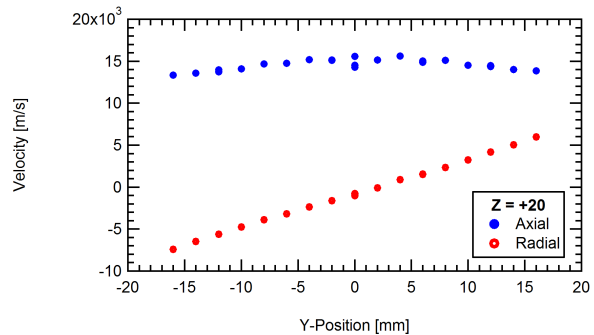


Figure 20. Axial and radial velocity profiles at $Z = +20$ mm for the off-nominal operating condition.

Plume Measurements

Figures 19 through 21 show the axial and radial velocity profiles in the plume of the CHT-30 under off-nominal operating conditions. As was seen in the nominal condition, the axial velocity field remains fairly constant across the thruster cross section. The radial velocity field, however, becomes more linear at greater distances into the plume. This is due to the reduced influence of the radial component of electric field farther from the exit plane.

At an axial position of $Z = +20$ mm, Figure 22 shows that the off-nominal condition has a higher centerline axial velocity than the nominal condition (15,600 m/s (166 eV) vs. 14,100 m/s (135 eV)). At this distance, however, the off-nominal condition with the lower magnetic field shows noticeably lower radial velocities at positions farther from the centerline (6,000 m/s (25 eV) vs 7,500 m/s (38 eV) at $Y = +16$ mm). It appears, therefore, that more of the applied potential is used to accelerate ions in the axial rather than radial direction for the off-nominal case.

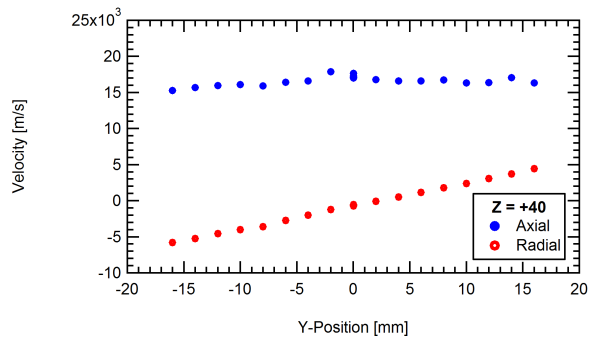


Figure 21. Axial and radial velocity profiles at $Z = +40$ mm for the off-nominal operating condition.

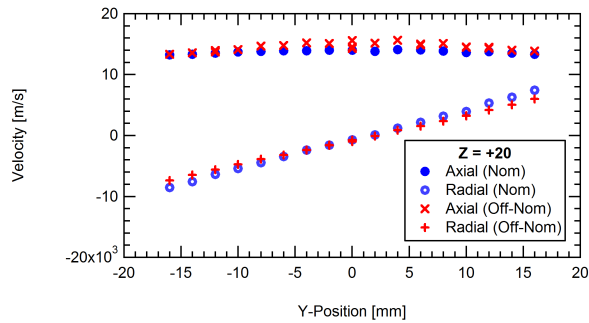


Figure 22. Comparison of nominal and off-nominal velocity profiles at $Z = +20$ mm.

Off-Nominal Condition at High Pressure

A second off-nominal condition was considered in order to examine the effect of increased chamber background pressure on the operation of the thruster. The background pressure was increased from 2.8×10^{-6} to 1.1×10^{-5} torr. This condition was chosen because the combination of reduced magnetic field strength and high background pressure increased the fluorescence signal strength, enabling measurements to be taken in the far-field of the plume. Measurements inside the thruster channel were not, however, taken at this operating condition.

Plume Measurements

Figure 23 shows the effect of increasing the chamber background pressure on the off-nominal operating condition. The higher background chamber pressure increases the axial velocity near the centerline of the thruster causing a more parabolic distribution across the channel, but causes little to no change in the radial velocity distribution. The resulting plume is more focussed, appearing to have a decreased plume divergence half angle and a peak acceleration region that is upstream (closer to the exit plane) compared to the low pressure cases. At $Z = +5$ mm, the cen-

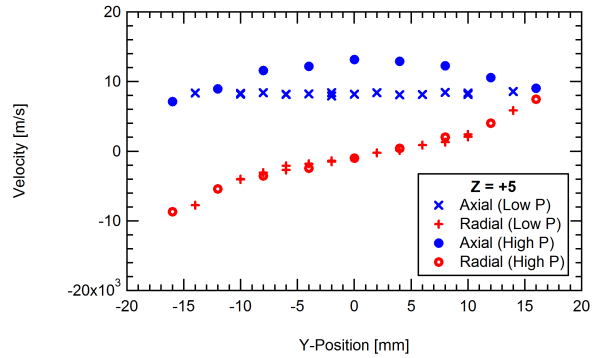


Figure 23. Comparison of off-nominal velocity fields at $Z = +5$ mm. Low P refers to the nominal 6×10^{-7} torr background pressure, whereas High P refers to 3×10^{-5} torr background pressure.

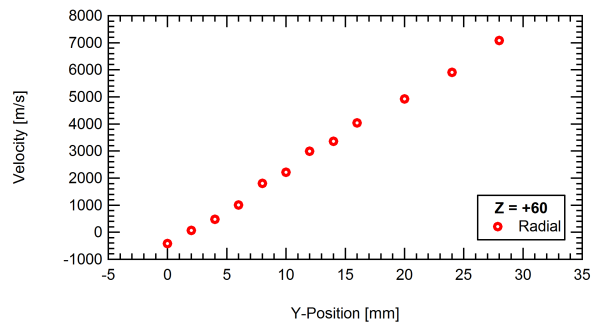


Figure 24. Velocity field at $Z = +60$ mm for nominal operating condition.

terline axial velocity is 13,200 m/s (118 eV) for the off-nominal condition at high pressure vs 8,200 m/s (46 eV) for off-nominal at low pressure.

Far-field Plume Measurements

Velocity measurements were also taken in the far-field of the plume, two channel radii from the exit plane at $Z = +60$ mm. At this position, the axial LIF signal was very weak, making it difficult to capture a distinct peak in the fluorescence signal. This was not, however, a problem in the radial direction where the signal strength was relatively strong. The radial velocity profile for the nominal operating condition at $Z = +60$ mm is shown in Figure 24. By reducing the magnet current and increasing the background pressure, fluctuations in the thruster operation decreased. This made the signal less noisy in the far-field of the plume. The increased SNR made it possible to infer axial velocities from the data at $Z = +60$ mm.

Examining Figure 25, it is possible to see that the CHT-30 achieves a peak axial velocity of 17,400 m/s (197 eV) for the off-nominal, high pressure condition. This shows that the maximum velocity at high

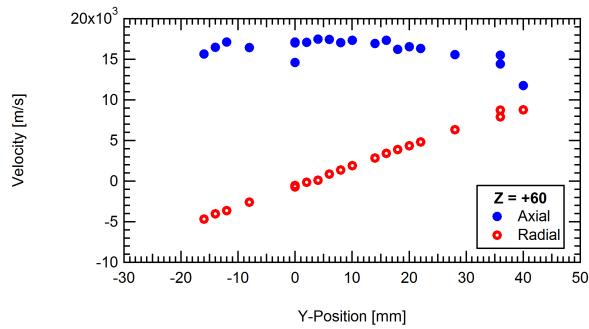


Figure 25. Off-nominal velocity field at $Z = +60$ mm with high background pressure.

pressure is slightly lower than the nominal condition, which reached 17,700 m/s (213 eV) by $Z = +40$ mm. It also shows that a good portion of the applied 300 V potential has been used to accelerate the xenon ions, and the acceleration continues into the far-field of the plume.

Comparison of Ion Acceleration Regions

Figure 26 shows the ion kinetic energy distribution at the centerline of the thruster channel for the nominal and two off-nominal conditions. A smoothing spline was used to interpolate the kinetic energy data, which was then differentiated to determine the axial electric field in the thruster channel and plume, as shown in Figure 27. The electric field profile is used to determine regions of acceleration in the thruster channel and plume.

Previous studies on the CHT showed that the majority of the xenon propellant is ionized at the border of the annular and cylindrical region. The ion acceleration then occurs in the cylindrical region of the channel, along which the greatest potential drop occurs.¹⁵ However, comparing the centerline velocities achieved inside the channel to those achieved outside shows that a large portion of the axial acceleration occurs in the thruster plume where the axial velocity reaches upwards of 17,000 m/s. This is confirmed by Figure 27, where the electric field acting on the ions is strongest in the plume between $Z = +10$ and $+20$ mm for the low chamber pressure cases.

Additionally, this shows good agreement with previous investigations of background effects on ion acceleration.¹⁹ It was shown that in an annular Hall thruster, an increase in background pressure pushes the ion acceleration region upstream.¹⁹ This is clearly visible in Figure 27, where for the high pressure case, the electric field is very high near the channel exit plane.

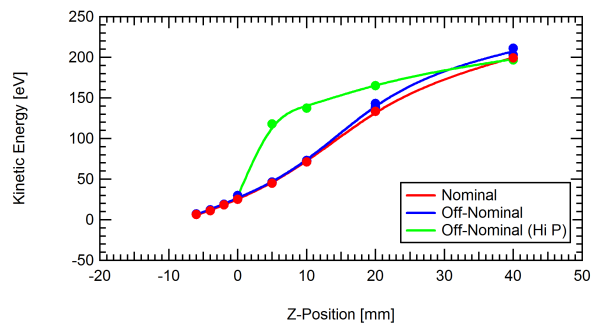


Figure 26. Ion kinetic energy profile at centerline of thruster ($X = 0$, $Y = 0$).

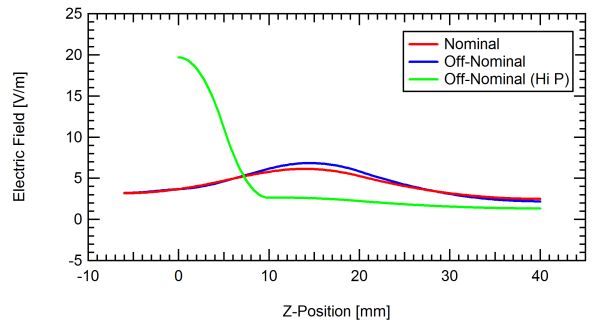


Figure 27. Electric field profile at centerline of thruster ($X = 0$, $Y = 0$).

Azimuthal Velocities

Measurements were also taken of the azimuthal drift velocity. This was accomplished by measuring the fluorescence signal excited by the vertical laser beam as it scanned across the X - Z plane.

Within the uncertainty of the measurement (± 500 m/s), it was shown that there is little to no azimuthal velocity. In the plume at a distance of $Z = +10$ mm, the azimuthal velocity measures zero to 225 m/s from the centerline of the thruster to the edge of the channel. However, beyond this point, there appears to be no distinct azimuthal velocity. It is likely that any azimuthal $E \times B$ drift in the thruster would be seen near the anode in the annular, ionization portion of the channel which contains a radial magnetic field, and it diminishes farther into the plume.

This is not surprising due to the magnetic field configuration of the CHT-30. Unlike a traditional Hall thruster, there is no center magnetic pole in the acceleration portion of the thruster channel to create a radial magnetic field. Instead, the magnetic field is produced by two electromagnets along the outer wall of the insulator, alternating in polarity to create a cusped magnetic field which has been shown to be mostly in the axial direction. This eliminates azimuthal Hall drift velocity caused by the $E \times B$ force

on the ions seen in the acceleration channel.

The azimuthal $E \times B$ drift strongly influences electron transport in conventional Hall effect thrusters. The lack of drift velocity and significantly different magnetic field topology implies that the electron transport mechanism in cusped field thrusters is very different from that of traditional Hall thrusters. Simulations and further measurements are needed to better understand this transport phenomena.

Conclusions

Laser induced fluorescence was used to map the ion velocities of the CHT-30 both inside the thruster channel and in the plume. A nominal operating condition was examined and compared to an off-nominal case with a weaker magnetic field at two chamber operating pressures. Results show that inside the thruster channel, the magnetic field profile prevents high energy ions from residing near the channel wall. Instead, these ions are focused toward then thruster centerline.

Once outside the thruster channel, the plume flow is highly divergent. The divergent profile is slightly mitigated by reducing the magnetic field strength and more so by increasing the chamber background pressure. Both cases resulted in a higher axial ion velocity than the nominal operating condition.

Under nominal operating conditions, the centerline axial velocity at the exit plane is 6,100 m/s (25 eV). The CHT-30 achieves an axial velocity of 17,700 m/s (213 eV) by +40 mm into the plume. This corresponds to a gain of approximately 188 eV in the plume, showing that there is a significant amount of acceleration outside of the chamber, more so than typical annular Hall thrusters.

The CHT-30 also differs from conventional Hall thrusters in that it has no azimuthal $E \times B$ drift velocity in the plume. This implies that electron transport in cusped field thrusters is different from that seen in conventional Hall effect thrusters.

There is still much to be learned about cylindrical Hall thrusters. While the scope of this paper was limited to surveying the most probable velocities at various points in the thruster discharge, further examination of the LIF data will enable the derivation of velocity distribution functions at these positions. Future studies on the CHT-30 also includes performing LIF measurements while running the cathode with enhanced electron emission in order to see the effect of reduced plume divergence on ion energy distributions and acceleration.² Finally, further modeling and experimental work are needed to understand electron transport mechanisms in cusped field thrusters.

Acknowledgments

The authors would like to thank D. L. O'Malley for his assistance in taking data, S. R. Gildea for his discussions about cusped field thrusters, and also Dr. C. W. Larson for sharing his knowledge of cylindrical Hall thrusters.

References

- ¹Hargus Jr., W. A. and Nakles, M. R., "Ion Velocity Measurements within the Acceleration Channel of Low-Power Hall Thruster," *IEEE Transactions on Plasma Science*, Vol. 36, No. 5, October 2008, pp. 1989–1997.
- ²Raitses, Y., S. A. and Fisch, N. J., "Enhanced performance of cylindrical Hall thrusters," *Applied Physics Letters*, Vol. 90, No. 221502, 2007.
- ³Hargus Jr., W. A. and Cappelli, M. A., "Laser-Induced Fluorescence Measurements of Velocity within a Hall Discharge," *Applied Physics B*, Vol. 72, No. 8, June 2001, pp. 961–969.
- ⁴Geisen, H., Krumpelmann, T., Neuschafer, D., and Ottinger, C., "Hyperfine Splitting Measurements on the 6265 Angstrom and 6507 Angstrom Lines of Seven Xe Isotopes by LIF on a Beam of Metastable Xe(3P0,3) Atoms," *Physics Letters A*, Vol. 130, No. 4-5, July 1988, pp. 299–309.
- ⁵Fischer, W., Huhnermann, H., Kromer, G., and Schafer, H. J., "Isotope Shifts in the Atomic Spectrum of Xenon and Nuclear Deformation Effects," *Z. Physik*, Vol. 270, No. 2, January 1974, pp. 113–120.
- ⁶Bronstrom, L., Kastberg, A., Lidberg, J., and Mannervik, S., "Hyperfine-structure Measurements in Xe II," *Physical Review A*, Vol. 53, No. 1, January 1996, pp. 109–112.
- ⁷Manzella, D. H., "Stationary Plasma Thruster Ion Velocity Distribution," *Proceedings of the 30th Joint Propulsion Conference and Exhibit*, No. AIAA-1994-3141, American Institute of Aeronautics and Astronautics, June 1994.
- ⁸Hansen, J. E. and Persson, W., "Revised Analysis of Singly Ionized Xenon, Xe II," *Physica Scripta*, , No. 4, 1987, pp. 602–643.
- ⁹Demtroder, W., *Laser Spectroscopy: Basic Concepts and Instrumentation*, Springer-Verlag, 1996.
- ¹⁰Miller, M. H. and Roig, R. A., "Transition Probabilities of Xe I and Xe II," *Physical Review A*, Vol. 8, No. 1, July 1973, pp. 480–486.
- ¹¹Moore, C. E., *Atomic Energy Levels*, Vol. II, National Bureau of Standards, 1958.
- ¹²Raitses, Y., S. A. and Fisch, N. J., "Cylindrical Hall Thrusters," *Proceedings of the 37th AIAA Plasmadynamics and Lasers Conference*, No. AIAA-2006-3245, American Institute of Aeronautics and Astronautics, June 2006.
- ¹³Smirnov, A., R. Y. and Fisch, N. J., "Enhanced Ionization in the Cylindrical Hall Thruster," *Journal of Applied Physics*, Vol. 94, No. 2, 2003.
- ¹⁴Gildea, S. R., B. and Martinez-Sanchez, M., "Fully Kinetic Modeling of Divergent Cusped-Field Thrusters," *Proceedings of the 45th Joint Propulsion Conference and Exhibit*, No. AIAA-2009-4814, American Institute of Aeronautics and Astronautics, August 2009.
- ¹⁵Smirnov, A., R. Y. and Fisch, N. J., "Experimental and Theoretical Studies of Cylindrical Hall Thrusters," *Physics of Plasmas*, Vol. 14, No. 057106, 2007.

¹⁶Kaufman, H. R., R. R. S. and Seddon, R. I., “End-Hall ion source,” *Vacuum Science & Technology A*, Vol. 5, No. 2081, 1987.

¹⁷Hargus Jr., W. A., , and Charles, C. S., “Near Exit Plane Velocity Field of a 200-Watt Hall Thruster,” *Journal of Propulsion and Power*, Vol. 24, No. 1, 2008, pp. 127–133.

¹⁸Raitses, Y., S. A. and Fisch, N. J., “Effects of enhanced cathode electron emission on Hall thruster operation,” *Physics of Plasmas*, Vol. 16, No. 057106, 2009.

¹⁹Nakles, M. R. and Hargus Jr., W. A., “Background Pressure Effects on Internal and Near-field Ion Velocity Distribution of the BHT-600 Hall Thruster,” AIAA, Preprint (2009).

IEPC-2009-XXXX

Laser Induced Fluorescence Velocity Measurements of a Cylindrical Hall Thruster



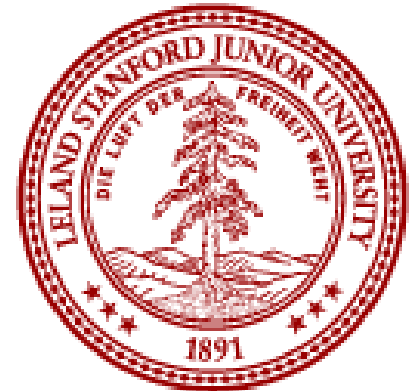
Natalia A. MacDonald

Mark A. Cappelli

*Stanford Plasma Physics Laboratory
Stanford University
Stanford, CA*

William A. Hargus, Jr.

*Spacecraft Propulsion Branch
Air Force Research Laboratory
Edwards Air Force Base, CA*





Introduction



Motivation

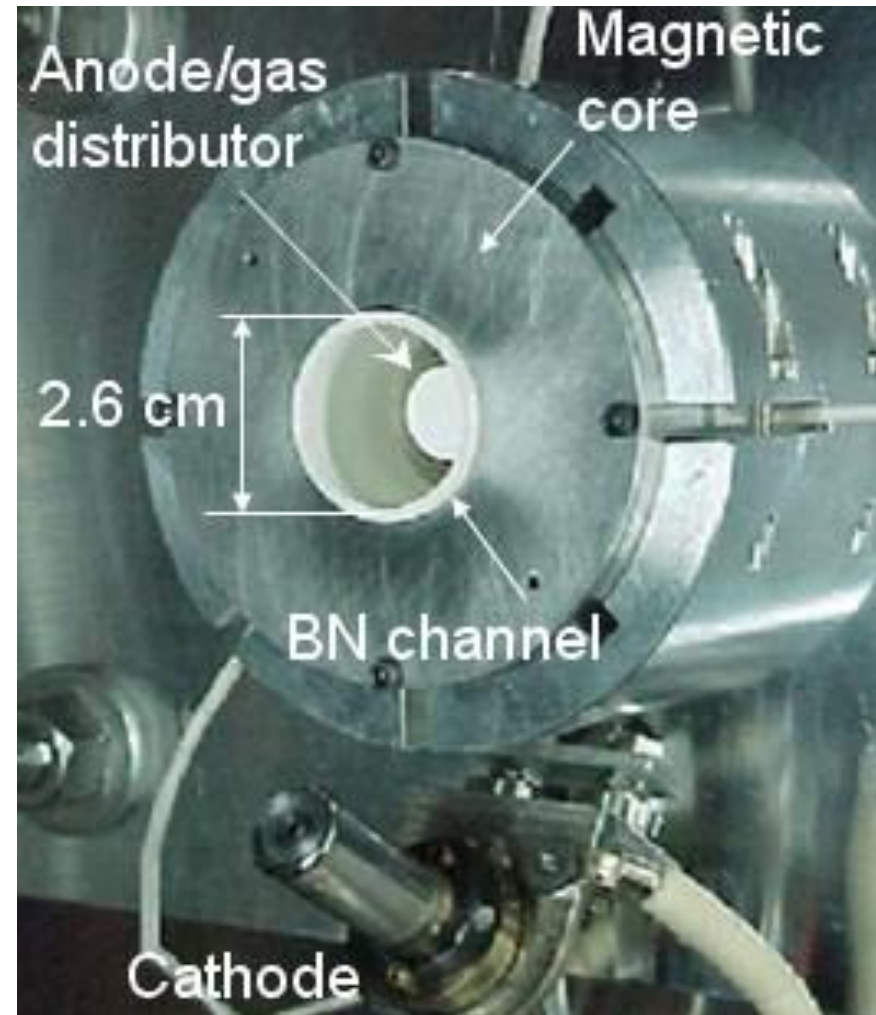
- Understand the Princeton University Cylindrical Hall Thruster (CHT-30)

Study Objectives

- Evaluate the effects of background pressure and magnetic field strength on ion acceleration.

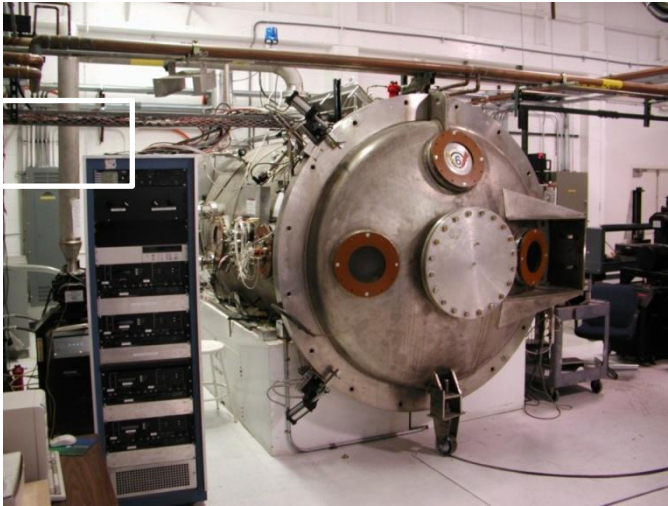
Methodology

- Characterize the internal ion velocity distribution using LIF
- Make measurements for two background pressures and two magnetic field configurations
- Estimate axial electric field in acceleration region based ion velocity measurements.

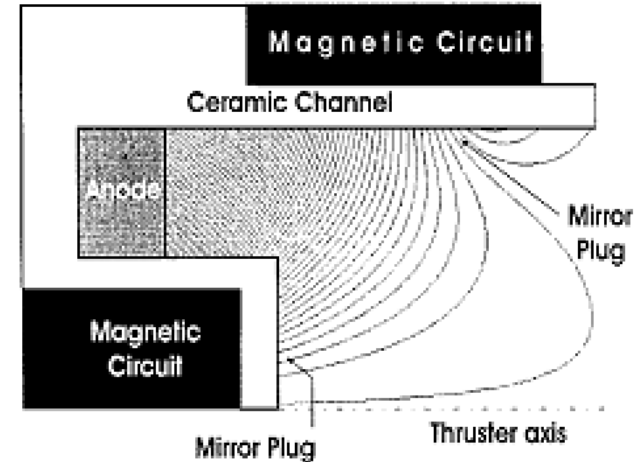




Testing Facilities and Cylindrical Hall Thruster



- AFRL Chamber 6, Edwards AFB
- Cryogenic pumping
 - 5 independent pumps
 - 32,000 L/s
- Stainless Steel chamber walls
 - 1.8 m diameter, 3.0 m length
 - Carbon beam dump



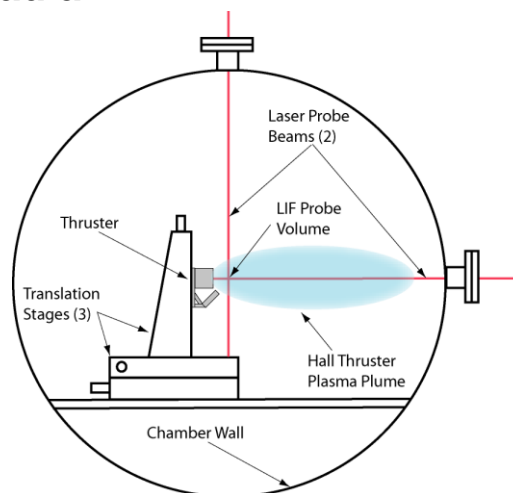
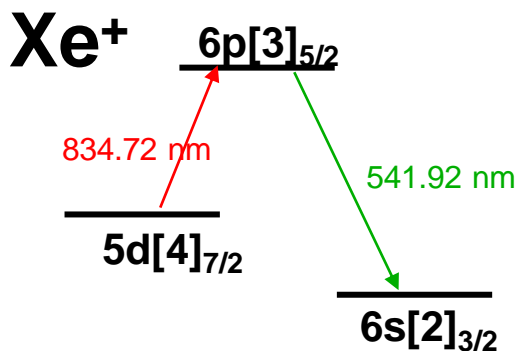
- Princeton University CHT-30
- Cylindrical cusp-type electrostatic thruster
 - Two electromagnets used to create cusped magnetic field profile
 - 30 mm diameter channel
 - 13 mm depth cylindrical portion of channel



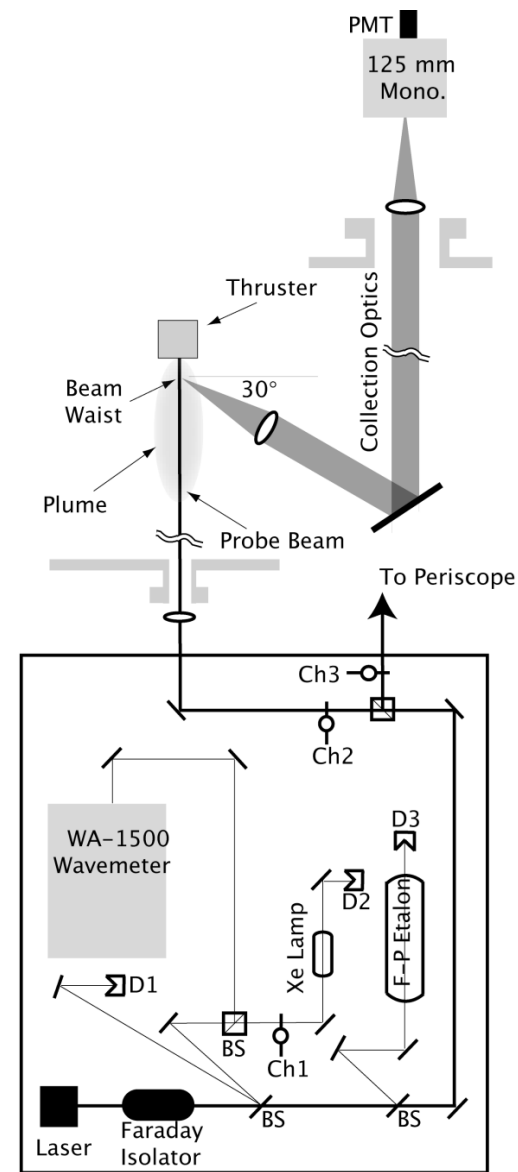
Experimental Apparatus



- Diode laser system with phase sensitive detection
 - New Focus Vortex [®] tunable diode laser (10 mW)
 - Simultaneous two axis velocity measurement
- Stationary Reference
 - Hollow cathode lamp
 - Non-resonant fluorescence collection using $6s[2]_{3/2} - 6p[3]_{5/2}$ neutral transition
 - Shifted 17.7 GHz from ionic line center
- Collection Optics
 - Resolution: Axial 1.0 mm, Radial 1.7 mm
 - Phase sensitive detection



Distribution A: Distribution Unlimited

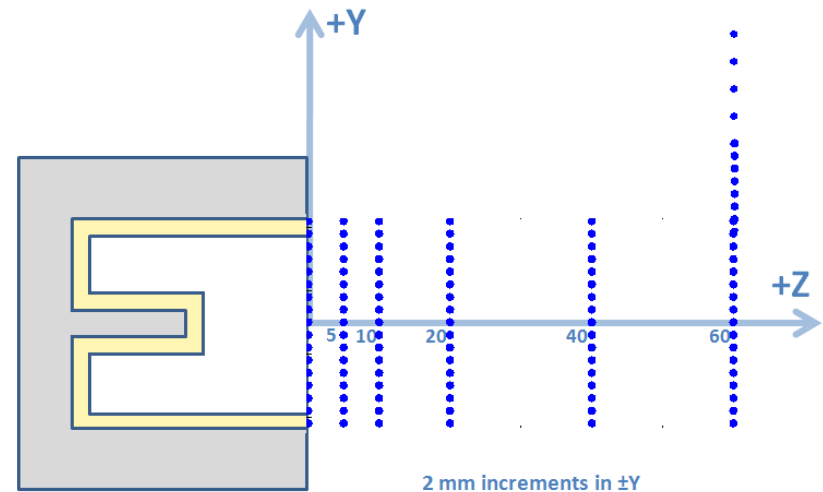
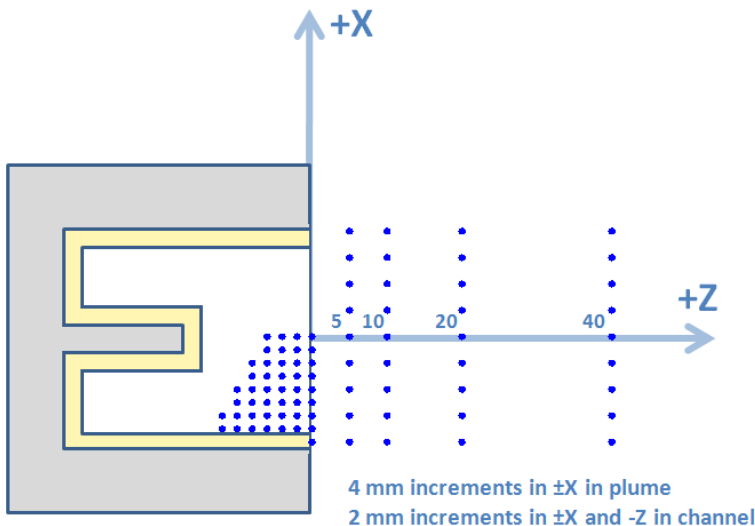
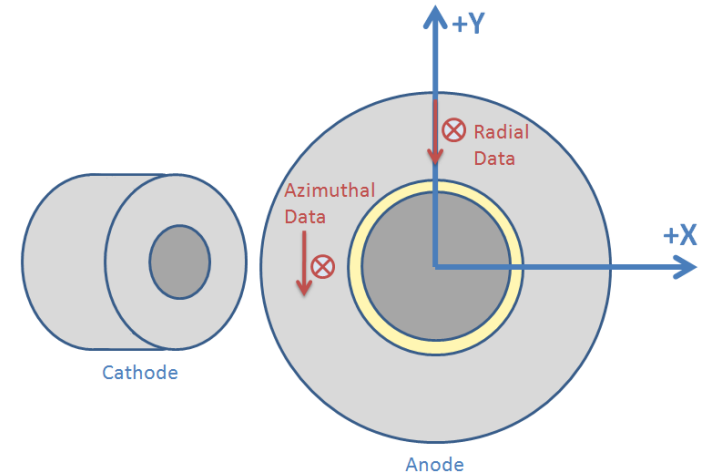




Data Points



- **Internal Measurements**
 - 2 mm increments in the X-Z plane
- **Plume Measurements**
 - 2 mm increments in the $\pm Y$ -direction
 - 4 mm increments in the $\pm X$ -direction
 - Axial positions of $Z = 0, +5, +10, +20, +40$ and $+60$ mm





Operating Conditions



- **Nominal case was chosen for comparison to unpublished performance data**
- **Off-nominal case was chosen to see the effect of differing magnetic field strengths**
 - Both the nominal and off-nominal cases were run at 2.8×10^{-6} torr
- **The off nominal case was also run at 1.1×10^{-5} torr to see the effect of background chamber pressure**

| Nominal Operating Condition | |
|-----------------------------|-------------------|
| Parameter | Measurement |
| Anode flow: | 390 μg |
| Cathode flow: | 98 μg |
| Anode potential: | 300 V |
| Anode current: | 0.53 A |
| Heater current: | 5.00 A |
| Keeper current: | OFF |
| Magnet #1 current: | 3.00 A |
| Magnet #2 current: | 2.00 A |

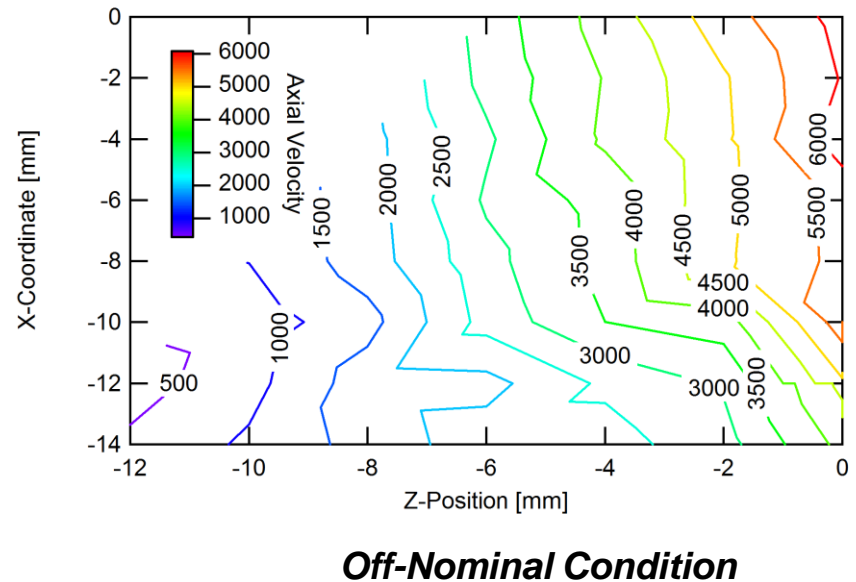
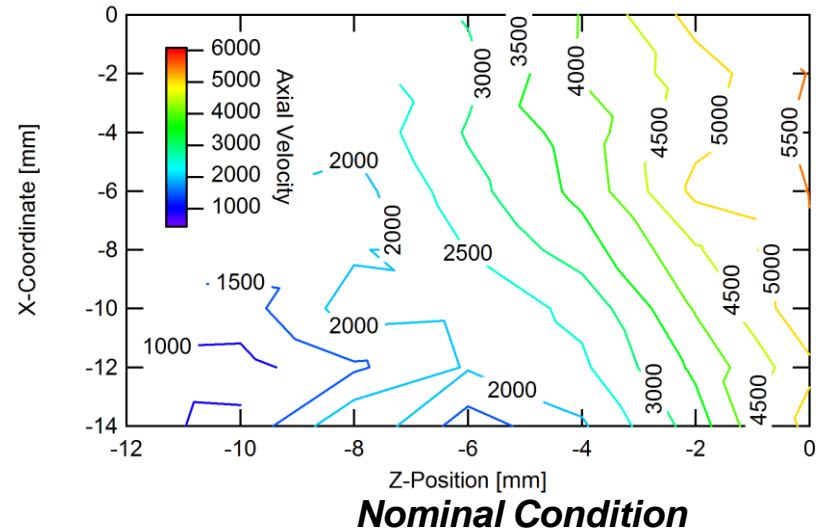
| Off-Nominal Operating Condition | |
|---------------------------------|-------------------|
| Parameter | Measurement |
| Anode flow: | 390 μg |
| Cathode flow: | 150 μg |
| Anode potential: | 300 V |
| Anode current: | 0.61 A |
| Heater current: | 5.00 A |
| Keeper current: | 0.30 A |
| Magnet #1 current: | 2.00 A |
| Magnet #2 current: | 2.00 A |



Interior Measurements



- **Magnetic field profile keeps ions away from walls**
 - Electric field is perpendicular to the magnetic field lines
 - Convergent ion flux
 - Reduced erosion
- **Velocity fields**
 - Parabolic through acceleration channel
 - Nearly constant across exit plane
- **Lower magnetic field case achieves slightly higher axial velocity at exit plane**
 - **6,100 m/s (25 eV) nominal vs. 6,600 m/s (30 eV) off-nominal**

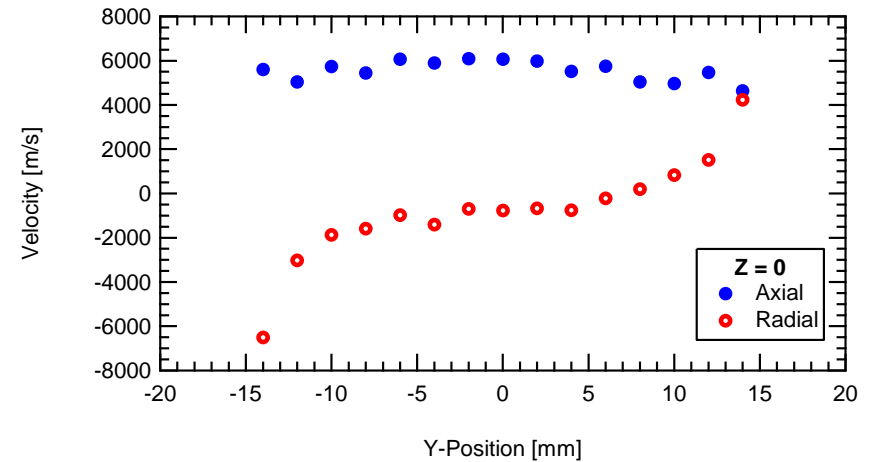




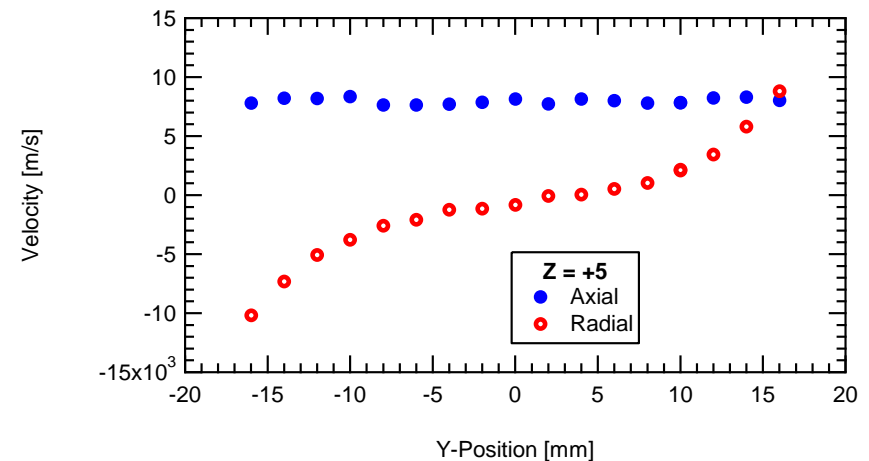
Plume Measurements (Nominal)



- **Exit plane velocities:**
 - Max axial velocity at centerline of channel = **6,100 m/s (25 eV)**
 - Max radial velocity at edge of channel = **6,500 m/s (29 eV)**
- **High radial ion velocity at the exit plane → large plume divergence half angle**
- **Axial velocity **17,700 m/s (213 eV)** at $Z = +40$ mm**
 - Ions gain significant velocity outside the thruster chamber



Nominal Velocities at Exit Plane



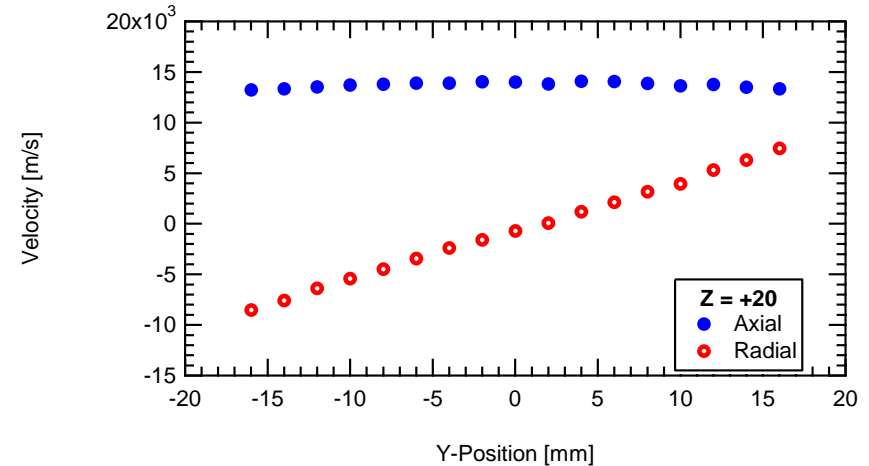
Nominal Velocities at $Z = +5$ mm



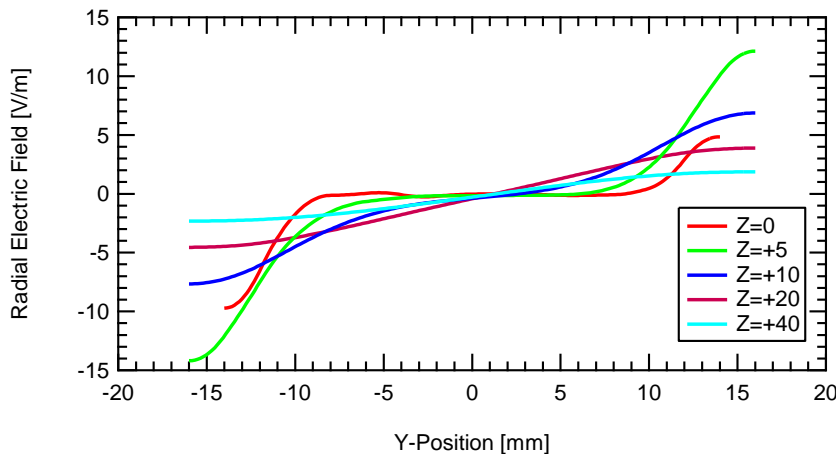
Plume Measurements (Nominal)



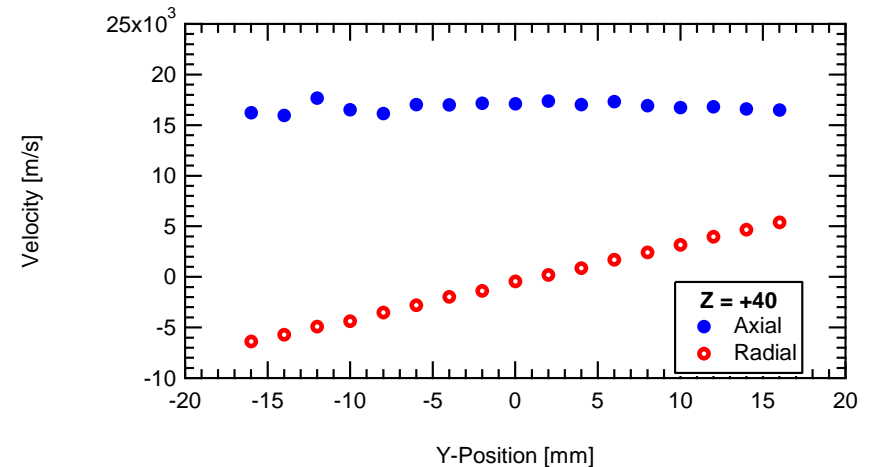
- Axial profile flattens out farther into plume
- Strong radial electric field near channel walls at exit plane
 - Ions may be magnetized
 - Influence of magnetic field is weaker farther into the plume



Nominal Velocities at $Z = +20$ mm



Radial Electric Fields for $Z = 0$ to $+40$ mm



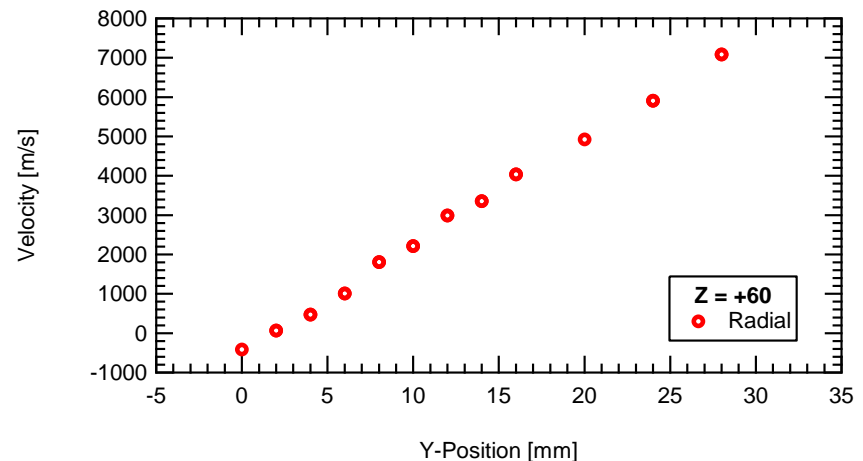
Nominal Velocities at $Z = +40$ mm



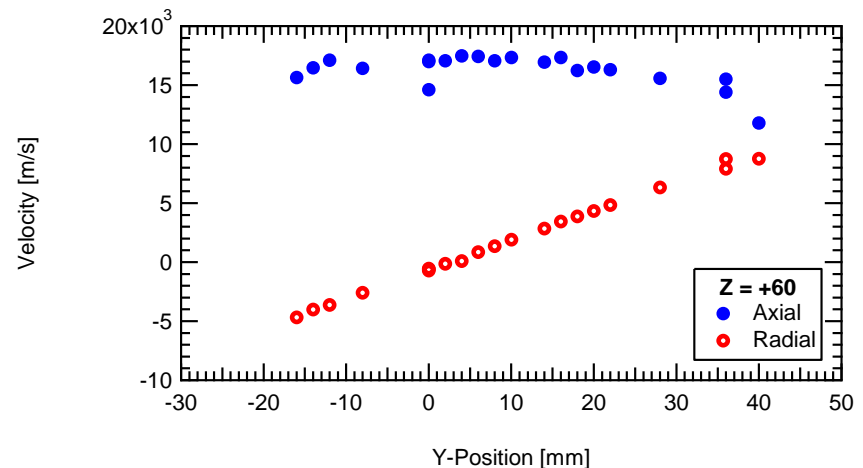
Far-field Plume Measurements



- Measurements made at $Z = +60$ mm
- Weak axial LIF signal for nominal conditions
 - Lowering magnetic field and raising background pressure enabled axial velocity measurement
- Radial signal is strong for both cases
- Maximum axial velocity for off-nominal, high pressure case is **17,400 m/s (197 eV)**
 - A good portion of the applied 300 V potential has been used to accelerate the xenon ions
- Acceleration continues into the far-field of the plume



Nominal Condition



Off-Nominal, High Pressure Condition



Plume Measurements (Off-Nominal)

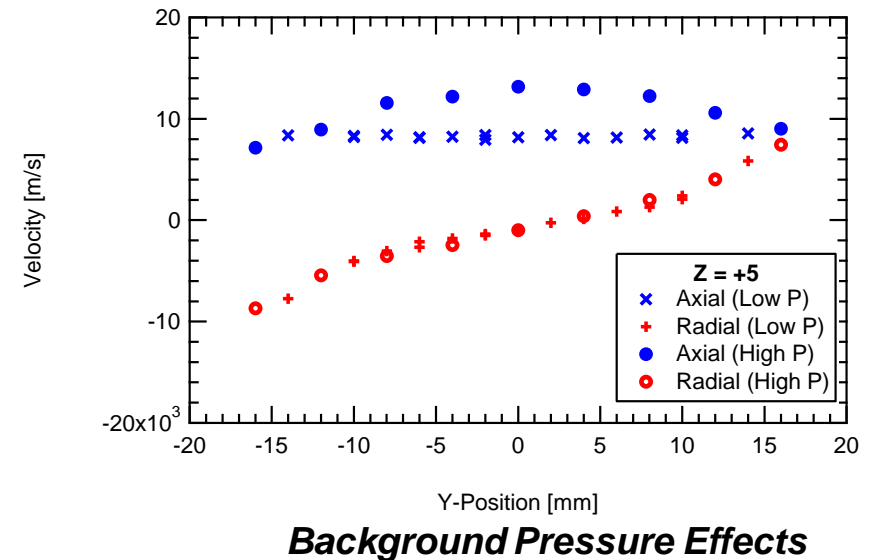
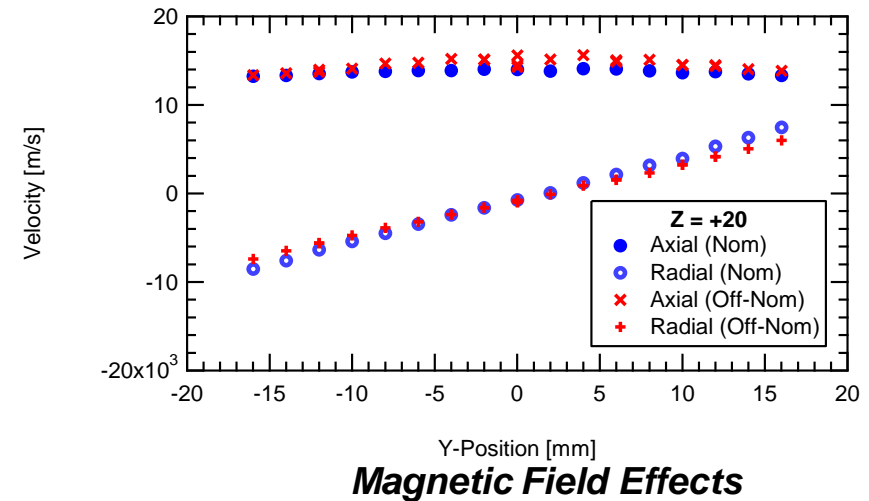


Magnetic Field Effects

- Higher centerline velocity than nominal condition
- Lower radial velocities than nominal condition

Background Pressure Effects

- Increased axial acceleration near centerline of channel
 - Parabolic axial velocity profile
 - Off-nominal at high pressure:
13,200 m/s (118 eV) at Z = +5 mm
 - Off-nominal at low pressure:
8,200 m/s (46 eV) at Z = +5 mm
- Radial velocity distribution shows no change
- Appearing to have a decreased plume divergence half angle

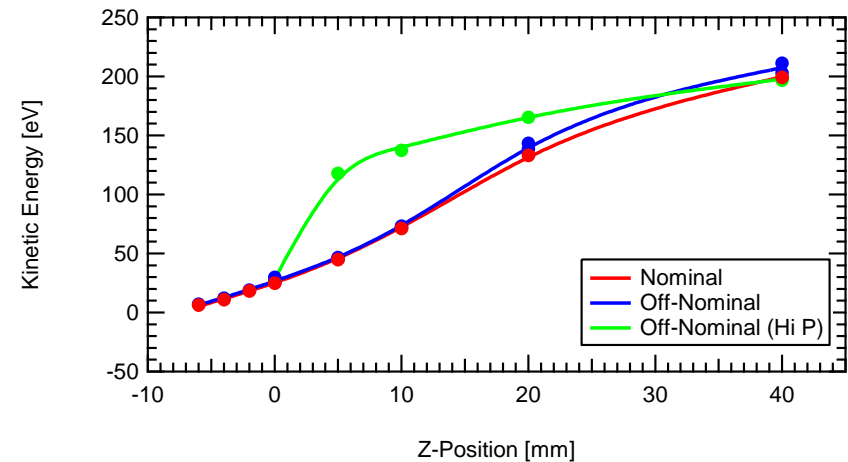




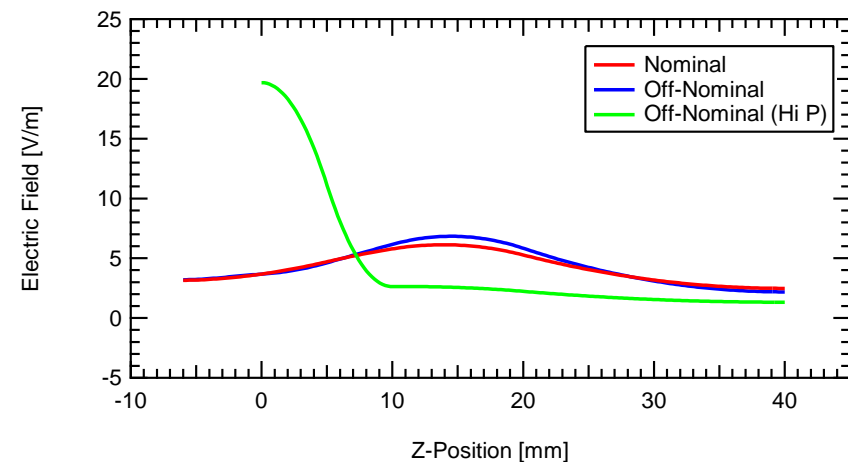
Comparison of Ion Acceleration Regions



- The majority of ion acceleration occurs in the plume
 - Ion velocities under nominal conditions:
 - At exit plane = 6,100 m/s (25 eV)*
 - At Z = +40 mm = 17,700 m/s (213 eV)*
- Peak electric fields:
 - Low chamber pressure cases:
 - Between Z = +10 and +20 mm*
 - High chamber pressure case:
 - Pushed upstream towards exit plane*



Centerline Kinetic Energy Distributions



Centerline Electric Field Distributions



Conclusions



- **Plume is highly divergent outside the thruster channel**
 - Less divergent with reduced magnetic field strength
 - Less divergent with increased background pressure
- **Significant acceleration is seen outside thruster channel**
 - 6,100 m/s axial velocity at exit plane (nominal)
 - 17,700 m/s axial velocity at $Z = +40$ mm (nominal)
 - Gain of 188 eV in plume (more than a traditional annular Hall thruster)



Future Work



- **Use LIF data to derive velocity distribution functions**
- **Better understand electron transport in cusp-type thrusters**
- **Take LIF measurements of CHT-30 while running cathode with enhanced electron emission**

Backup Slides



Xenon Laser-Induced Fluorescence: Neutral and Ionic Velocities



Neutral Xe (Xe I)

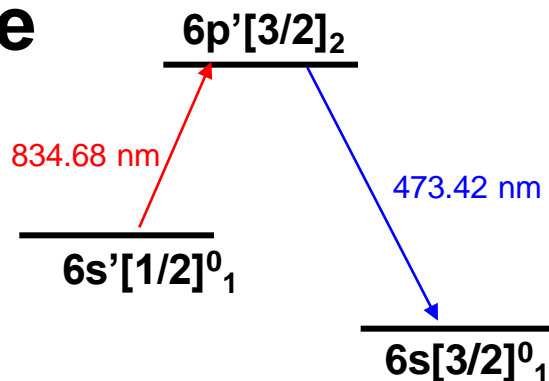
- Xenon neutral $6s'[1/2]_1^0 - 6p'[3/2]_2$ transition
 - Accessible (diode & Ti:Sapphire)
 - Previous use unknown...
 - Non-resonant fluorescence collection
 - Hyperfine spin splitting data unknown

Ionic Xe (Xe II)

- Xenon ion $5d[4]_{7/2} - 6p[3]_{5/2}$ transition
 - Accessible (diode & Ti:Sapphire)
 - Used previously for velocity measurements by various groups
 - Non-resonant fluorescence collection
 - Some hyperfine spin splitting data known

A single laser system with ± 50 GHz tuning range can be used to probe both ions and neutrals

Xe



**~18.1 GHz
Separation**

Xe⁺

